M Dwarfs From Hubble Space Telescope Star Counts III: The Groth Strip

Andrew Gould[⋆]

Dept of Astronomy, Ohio State University, Columbus, OH 43210

John N. Bahcall

Institute For Advanced Study, Princeton, NJ

Chris Flynn

Tuorla Observatory, Piikkiö, FIN-21500, Finland

e-mail: gould@payne.mps.ohio-state.edu, jnb@ias.edu, cflynn@astro.utu.fi

Abstract

We analyze the disk M dwarfs found in 31 new fields observed with the Wide Field Camera (WFC2) on the *Hubble Space Telescope (HST)* together with the sample previously analyzed from 22 WFC2 fields and 162 prerepair Planetary Camera (PC1) fields. The new observations, which include the 28 high-latitude fields comprising the Large Area Multi-Color Survey ("Groth Strip"), increase the total sample to 337 stars, and more than double the number of late M dwarfs ($M_V > 13.5$) from 23 to 47. The mass function changes slope at $M \sim 0.6 M_\odot$, from a near-Salpeter power-law index of $\alpha = -1.21$ to $\alpha = 0.44$. In both regimes the mass function at the Galactic plane is given by

$$\frac{d^3 N}{d \log M \, d\, M_V \, dV} = 8.1 \times 10^{-2} \mathrm{pc}^{-3} \left(\frac{M}{0.59\, M_\odot} \right)^{\alpha}$$

The correction for secondaries in binaries changes the low-mass index from $\alpha = 0.44$ to $\alpha \sim 0.1$. If the Salpeter slope continued to the hydrogen-burning limit, we would expect 500 stars in the last four bins ($14.5 < M_V < 18.5$), instead of the 25 actually detected. The explanation of the observed microlensing rate towards the Galactic bulge requires either a substantial population of bulge brown dwarfs or that the disk and bulge mass functions are very different for stars with $M \lesssim 0.5\, M_\odot$.

⋆ Alfred P. Sloan Foundation Fellow

Subject Headings: dark matter – gravitational lensing – stars: low mass, luminosity function

submitted to *The Astrophysical Journal*: November 20, 1996
Preprint: OSU-TA-31/96

1. Introduction

We present new results from a search for M dwarfs found in images taken using the *Hubble Space Telescope (HST)*. The primary aim of this program is to measure the faint end of the disk luminosity function (LF), and thus to address four questions: What is the contribution of M stars to the disk mass? Is the disk mass function (MF) rising at the last measured point which would indicate the possible presence of brown dwarfs beyond the hydrogen-burning limit? What is the vertical distribution of the disk? What contribution do disk stars make to the observed microlensing events?

In Paper I (Gould, Bahcall, & Flynn 1996) we analyzed a total of 257 M dwarfs, 192 in 22 fields imaged with the repaired Wide Field Camera (WFC2) with mean limiting mag $I = 23.7$ and 65 stars in 162 fields imaged with the prerepair Planetary Camera (PC1) with mean limiting mag $V = 21.3$. Our principal result was that the disk LF peaks at $M_V \sim 12$ and correspondingly that the disk MF (per unit log mass) peaks at $M \sim 0.5\, M_\odot$.

Here we combine these previous results with 80 additional M dwarfs found in 31 WFC2 fields of which 28 slightly overlapping fields comprise the Large Area Multi-Color Survey ("Groth Strip", $l = 96°$, $b = 60°$). The Groth Strip is at substantially higher latitude than the typical field analyzed in Paper I, and therefore the mean number of stars per field in the new sample is substantially smaller (2.6 vs. 8.7). However, high-latitude fields are relatively more sensitive to intrinsically fainter stars, so the additional 31 new fields more than double the number of late M dwarfs ($M_V > 13.5$) in the sample from 23 to 47. Since the determination of the LF is mainly limited by small number statistics at the faint end, these additional fields permit a significant improvement in the measurement.

Our principal result is to confirm the break in the MF with our best estimate now at $M \sim 0.6$, and to quantify this break as a change in the power-law index from the near-Salpeter value of $\alpha = -1.21$ to $\alpha = 0.44$ ($\alpha = -1.2$ to $\alpha = 0.1$ after correction for binaries).

2. Observations and Analysis

Table 1 gives the characteristics of the 31 new WFC2 fields as well as those of the 22 fields analyzed in Paper I. The fields are listed in order of increasing Galactic latitude in each group. In Paper I we described our method for determinating the detection threshold ($I_{\rm max}$) and the saturation threshold ($I_{\rm min}$). Table 1 also gives the area of each field in units of the effective area of WFC2 ($4.4\,{\rm arcmin}^2$).

For most of the fields, the method used to identify and measure point sources is the same as in Paper I and is illustrated by figure 2b of Flynn, Gould, & Bahcall (1996). However, four of the fields (the first three listed in Table 1, plus one of the Groth Strip fields) are dithered and required a new method of analysis. This method is described by Flynn et al. (1996) and is illustrated by their figure 2a.

The transformations from instrumental to standard Johnson-Cousins mags are given by equation (2.1) of Bahcall et al. (1994). As in Paper I we adopt the color-mag relation of Reid (1991), $M_V = 2.89 + 3.37(V-I)$, with an error of 0.44 mag.

2.1. Comments on Specific Fields

Several fields have specific features that require comment. First, the Groth Strip ($l=96^\circ$, $b=60^\circ$) is a mosaic of 28 fields whose overall center is approximately given by the RA and Dec of row 4 in Table 1. Because of a slight (7.5%) overlap of neighboring fields, the total area is slightly less than 28 isolated fields. The magnitude limits are not precisely uniform over this field. There are sections each with 3.6% of the total area having detection thresholds that are 0.21, 0.20, 0.16, 0.16, and -1.16 mag brighter than the modal value listed in Table 1. There are also sections each with 3.6% of the total area having saturation thresholds that are 0.05 and -0.70 mag brighter than the modal value. These differences are taken into account in the analysis.

The actual saturation threshold of the Hubble Deep Field (HDF, $l=126^\circ$, $b=55^\circ$) is $I_{\rm min}=18.75$ (set by a minimum exposure of 1100 s). However, unlike all of the other fields in the sample, HDF was chosen as a "blank field" by first inspecting Palomar Observatory Sky Survey plates (Williams et al 1996). Thus, it is possibly biased against "bright" stars that would be visible in these images. We therefore choose a bright limit that is certainly fainter than the influence of such possible bias, but is at the same time not influenced by our knowledge of the stellar content of this particular field (as reported by Flynn et al. 1996). We choose the mode of the bright limits of the Paper I fields, $I_{\rm min}=19.45$, corresponding to a minimum exposure of 2100 s and to $V_{\rm min}>21$ for the M dwarf sample selected by $V-I>1.53$.

TABLE 1

WFC2 Fields

RA (2000)	Dec (2000)	l	b	$I_{\rm max}$	$I_{\rm min}$	Ω (WFC2)
New Observations						
17 14 14.88	+50 15 30.0	77	+36	24.72	19.42	0.90
15 58 49.18	+42 05 26.3	67	+49	24.95	19.45	1.00
12 36 49.40	+62 12 58.0	126	+55	25.67	19.45	1.00
14 16 31.98	+52 15 51.9	96	+60	23.79	18.75	25.98
Previous Observations						
21 51 17.91	+28 59 53.9	82	−19	23.46	18.09	1.00
21 51 34.68	+28 58 13.3	82	−19	23.59	18.84	1.00
04 24 55.56	+17 04 47.8	179	−22	22.83	17.65	1.00
06 52 43.16	+74 21 38.4	140	+26	23.98	19.45	0.67
07 42 41.12	+49 44 17.5	169	+28	23.98	19.45	1.00
07 42 44.66	+65 06 08.5	151	+30	23.98	19.45	1.00
00 49 06.99	+31 55 48.6	122	−31	23.98	19.45	1.00
14 42 16.61	−17 10 58.7	337	+38	23.73	17.05	1.00
16 01 22.24	+05 23 37.2	16	+40	23.37	18.64	1.00
00 29 05.46	+13 08 07.4	115	−49	24.07	19.45	1.00
03 49 58.89	−38 13 43.3	241	−51	24.40	17.89	1.00
14 13 11.78	−03 07 57.0	339	+54	23.22	18.53	1.00
15 19 41.20	+23 52 05.4	36	+57	24.26	18.84	1.00
12 55 41.55	−05 50 56.9	305	+57	23.84	19.45	1.00
01 44 10.61	+02 17 51.2	148	−58	23.74	19.45	1.00
14 45 10.26	+10 02 49.7	6	+58	22.91	17.34	1.00
02 56 22.03	−33 22 25.3	234	−62	23.98	19.45	1.00
13 38 18.49	+04 28 03.1	331	+65	23.40	17.50	1.00
01 10 03.01	−02 26 22.8	134	−65	23.58	19.45	1.00
01 09 59.79	−02 27 23.7	134	−65	23.83	19.45	0.67
14 34 51.89	+25 10 04.5	34	+67	23.92	18.64	1.00
01 17 07.71	−08 39 10.9	142	−71	22.56	17.89	1.00

Three fields have less than full area coverage. One chip (33% of the field) was unusable in the field at $l = 140°$, $b = 26°$. Ten percent of the field at $l = 77°$, $b = 36°$ was also unusable. One chip from the field at $l = 134°$, $b = -65°$ overlaps a neighboring field and is therefore excluded.

2.2. The Groth Strip

Work on star counts in the modern era has proceeded by analyzing relatively large fields each with many stars. The resulting color-magnitude diagrams can then be visually inspected and directly compared with results of the models constructed from all the fields. See Bahcall (1986) for a review. By contrast, in the present program we analyze many small fields scattered over the sky, most with very few stars. Indeed, 47 of the 162 PC1 fields contain no stars at all. Hence visual comparison with models is not usually fruitful. Because of its large size, the Groth Strip offers a unique opportunity to compare the model with a field having many stars.

In Figure 1, we plot absolute magnitude (inferred from the observed color: $M_V = 2.89 + 3.37[V - I]$), and height modulus above the plane ($\mu_z = V_0 - M_V + 5\log_{10}\sin b$). Here $V_0 = V$, since the extinction is $A_V = 0$ (Burstein & Heiles 1984). The diagram can be compared directly to figure 1 of Paper I. The diagonal lines represent the magnitude limits $I_{\rm min}$ and $I_{\rm max}$. The large box is the M dwarf selection function which is discussed in Paper I: $V - I > 1.53$ (to avoid contamination by spheroid giants), $V - I < 4.63$ (to avoid the region where the color-mag relation becomes double-valued), and $z < 3200\,$pc (to avoid contamination by spheroid dwarfs). The smaller rectangular figure at the top shows the LF (per 100 pc^3 per mag) taken from Figure 2, below. The rectangular figure at the right shows the vertical distribution as given by equation (3.2) and Table 2, below. The units are chosen so that the expected density of stars in the diagram is the product of the two numbers at the top and right. For example, for the 3 small boxes (each 1 mag^2), the LF is 1.0, and the height functions are 2.8, 4.2, and 5.0 respectively. Hence, the expected numbers of stars per box (or fraction of a box where the box goes past the mag limits) are 2.8, 4.2, and 5.0, respectively. With allowance for Poisson errors, the model is a good representation of the data.

The small box at the upper left of the main figure must contain only spheroid stars because if these were disk stars they would be 6 to 8 kpc above the plane. The observed kinetic energy of disk stars is insufficient to reach such heights. Using the spheroid LF of Dahn et al. (1995) and assuming that spheroid stars in this color range are 2.5 mag fainter than disk stars of the same color (Monet et al. 1992), we predict that this box should contain a total of $22f$ stars, where f is a number that depends on the spheroid flattening, c/a. For $c/a = 0.6$, 0.8, and 1, we find $f = 0.8$, 0.9, and 1. This compares with 19 stars actually in the box. We conclude that the Dahn et al. (1995) LF is consistent with the Groth Strip data.

In Paper I, we argued that with the adopted height limit $z < 3200$, contamination by spheroid dwarfs is negligible and can be ignored. We have now checked

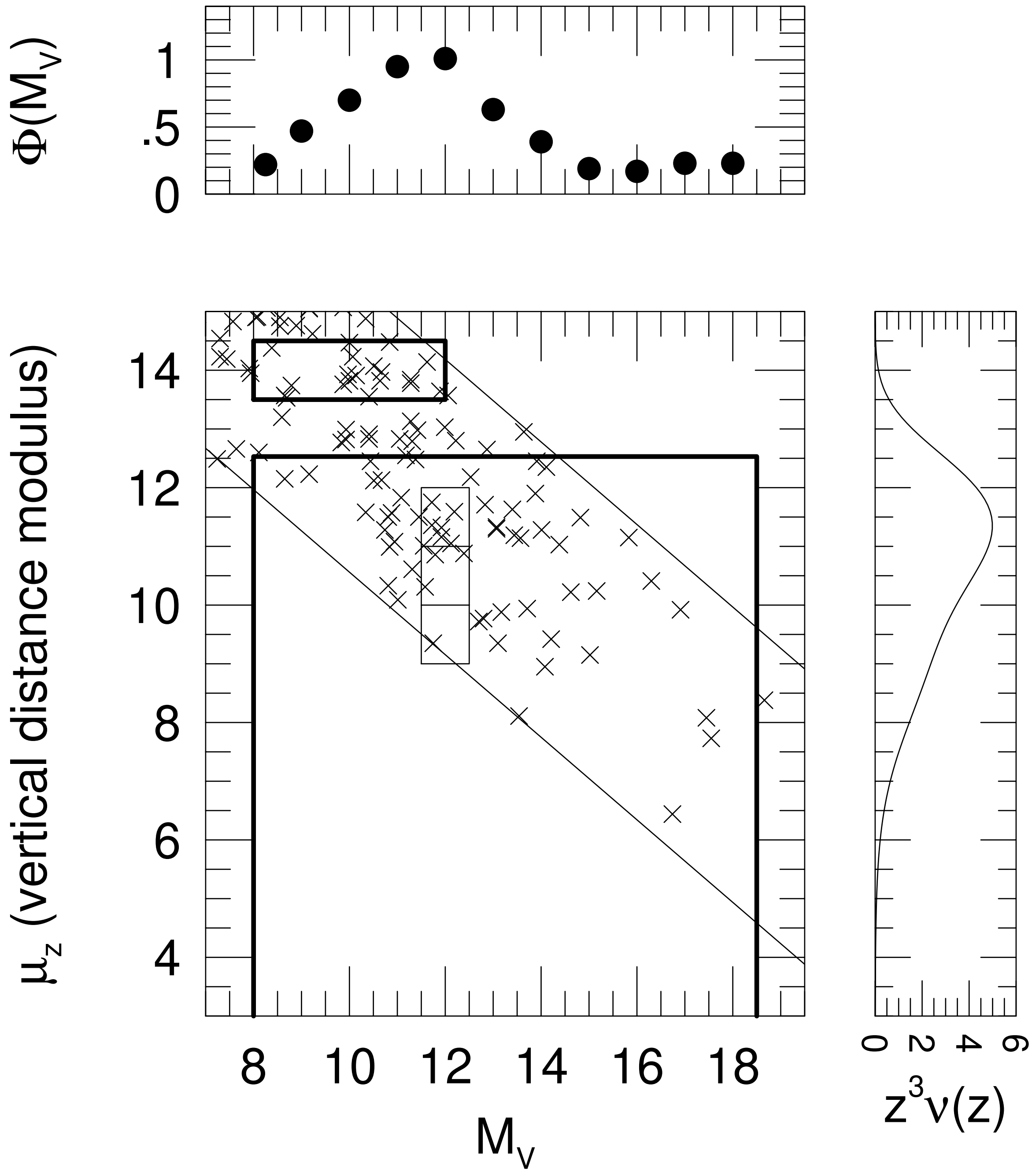

Figure 1. Stars in the Groth Strip shown by M_V (inferred from color) and height modulus above the plane ($\mu_z = V_0 - M_V + 5\log\sin b$). Diagonal lines represent the I-band range of sensitivity. Large box is selection function for M dwarfs described in text. The number of stars predicted in each 1 mag^2 box (such as the three small boxes at $M_V = 12$) are the product of the LF shown at the top (see Fig. 2) and the vertical density function at right (see eq. 3.2 and Table 2). Axis labels on the two smaller boxes are short-hand and omit factors of 100 and $2 \times 10^{-3}(\ln 10)\Omega \csc^3 b$ respectively. Small box at upper left contains only spheroid subdwarfs. The actual number in the small box (19) is in good agreement with the model of Dahn et al. (1995), which predicts 20 ± 5 stars in the box (see text).

that this is correct by incorporating into our models the spheroid stars expected on the basis of the Dahn et al. (1995) LF. We find that indeed the effects are much smaller than the Poisson errors, typically $\mathcal{O}(1\%)$. We therefore ignore spheroid contamination of the disk star region.

3. Results

3.1. Models

We model the distribution of stars as a function of Galactic position and absolute magnitude by,

$$\Phi(i,z,R) = \Phi_i \nu(z) \mathrm{exp}\left(-\frac{R-R_0}{H}\right), \tag{3.1}$$

where Φ_i is the LF at the Galactic plane for the ith magnitude bin, (R,z) is the Galactic position in cylindrical coordinates, $R_0 = 8\,\mathrm{kpc}$ is the solar galactocentric distance, and H is the disk scale length. We consider two forms for the vertical distribution function $\nu(z)$, the "sech^2" distribution

$$\nu_s(z) = (1-\beta)\mathrm{sech}^2\frac{z}{h_1} + \beta\,\mathrm{exp}\frac{-|z|}{h_2}, \tag{3.2}$$

and the "double exponential" distribution

$$\nu_e(z) = (1-\beta)\mathrm{exp}\frac{-|z|}{h_1} + \beta\,\mathrm{exp}\frac{-|z|}{h_2}. \tag{3.3}$$

The LF is assumed constant within each of the nine luminosity bins centered at $M_V = 8.25$ (1/2 mag), $M_V = 9$, 10, 11, 12, 13, and 14 (1 mag), and $M_V = 15.50$ and 17.50 (2 mag). (Later we also break up the last two bins into four 1-mag bins.) Thus, the fit has a total 13 parameters including nine LF parameters plus H, β, h_1, and h_2.

3.2. Global Parameters

We found in Paper I that the LF's for the sech^2 and double exponential fits were nearly identical up to an overall factor of 1.93 and that for heights $z \gtrsim 300\,\mathrm{pc}$, $\Phi_{i,s}\nu_s(z)$ was nearly identical to $\Phi_{i,e}\nu_e(z)$. That is, the only difference between the two distributions was the relative normalization near the plane. Since the sample contains almost no stars in this region (see fig. 1 from Paper I and also Fig. 1), we could not distinguish between these models on the basis of the *HST* data alone. We therefore fixed the local normalization according to the LF determined from local parallax stars (Reid, Hawley, & Gizis 1995) in the region $8.5 \leq M_V \leq 12$ where all previous studies of the LF agree. We then formed a linear combination of the two models to reproduce this density. In fact, the sech^2 model agreed almost perfectly with the local parallax normalization and therefore was in effect the adopted model. With the present expanded data set we again find that the sech^2 model agrees with the parallax-star normalization to within 1%. We therefore simply adopt the sech^2 distribution and dispense with linear interpolation.

Table 2 compares the best-fit parameters of the model using all the available data with the previous values determined in Paper I. The present and previous disk parameters are in excellent agreement. Here ρ_0 is the mass density of M dwarfs at the plane and Σ_M is the column density of M dwarfs.

TABLE 2

Best-Fit Sech^2 Models for M Stars ($8 < M_V < 18.5$)

Data Set	h_1 (pc)	h_2 (pc)	β	ρ_0 ($M_\odot \mathrm{pc}^{-3}$)	Σ_M ($M_\odot \mathrm{pc}^{-2}$)	H (kpc)
Present	320 ± 50	643 ± 60	$21.6 \pm 6.8\%$	0.0158 ± 0.0041	12.3 ± 1.8	2.92 ± 0.40
Previous	323 ± 54	656 ± 78	$19.8 \pm 7.1\%$	0.0159 ± 0.0044	12.4 ± 1.9	3.02 ± 0.43

3.3. Luminosity Function

It is not surprising that the global parameters change very little: the total number of stars has increased by only 31%. Of greater interest is the faint end of the LF ($13.5 < M_V < 18.5$) whose determination depended previously on only 23 stars and for which there are now 47. Figure 2 shows the present (triangles) and previous (circles) determinations of the LF. The new data basically confirm the previous results.

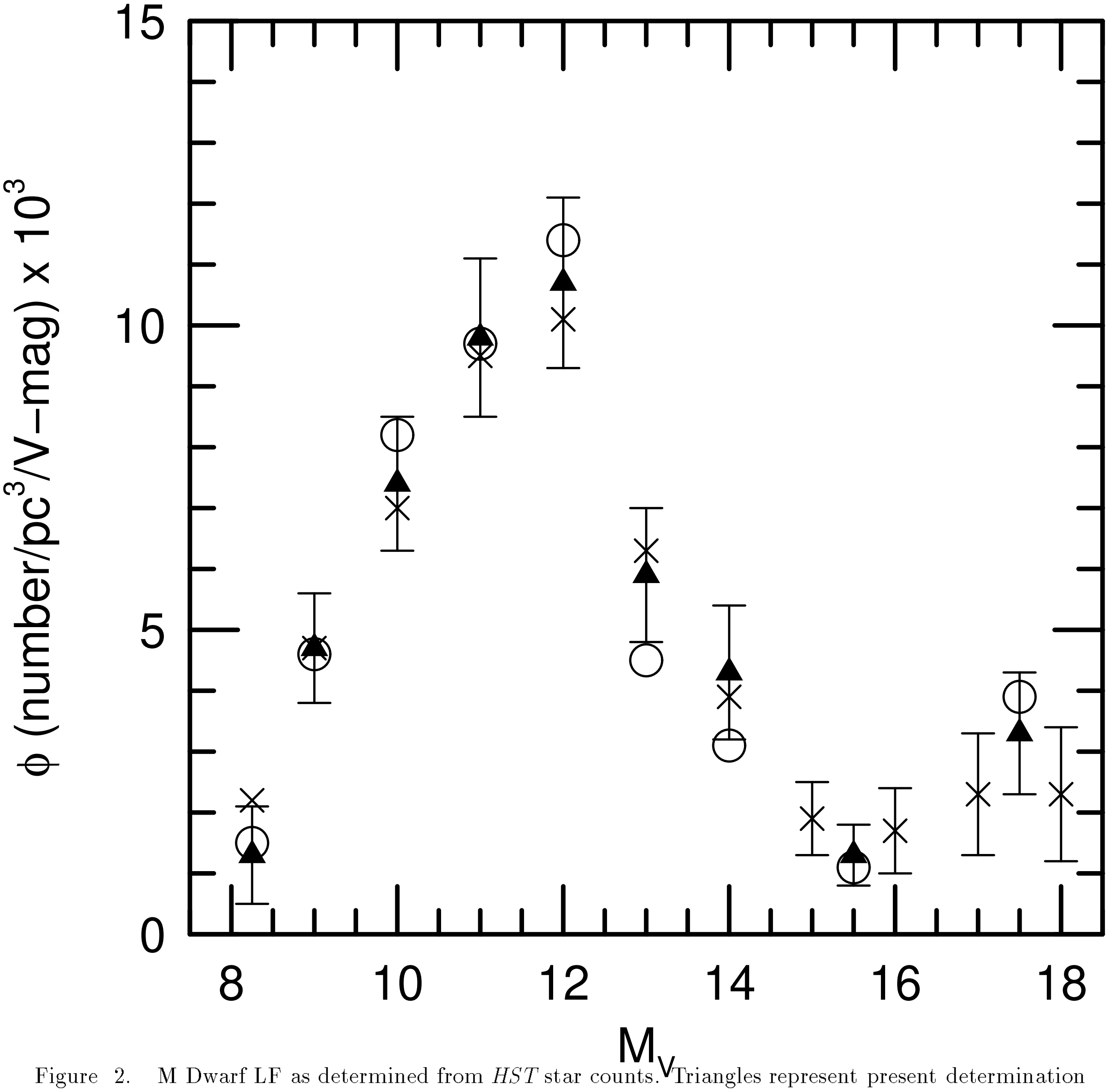

Figure 2. M Dwarf LF as determined from *HST* star counts. Triangles represent present determination using maximum likelihood (ML) method including error bars determined within the fit. Circles represent the LF as determined in Paper I by the same method. Error bars not shown for these to avoid clutter. As discussed in text, ML can amplify small scale structure caused by Poisson fluctuations. We therefore also show (crosses) the LF as determined by naive binning of star counts, a method which does not have this problem. Error bars for the naive-binning LF are shown only for the last four points.

However, we have discovered a subtle interplay between statistical and systematic effects which could affect the interpretation of the final two points ($M_V = 15.5$ and 17.5). The maximum likelihood fitting procedure (described in detail in Paper

I) takes account of both measurement errors and scatter of the absolute magnitudes (Malmquist bias). If the fitting procedure finds that the counts in one bin are depressed relative to the bins on *both* sides, it will conclude that the intrinsic density in this bin is *even lower* because more stars will have been scattered into than out of the bin. Thus, it will tend to further depress the LF at $M_V = 15.5$ and raise it at $M_V = 17.5$. If the depression at $M_V = 15.5$ is real (and not simply a statistical fluctuation) and if the error estimates are accurate, this will lead to a more accurate estimate of the LF at this bin. However, this bin contains a total of only 15 stars, and the final bin contains only 10. Thus, the alternative explanation of a statistical fluctuation is also plausible.

To investigate this possibility further, we make the following alternative estimate of the LF. We first calculate the effective volume, $v_{\text{eff},j}(M_V)$, as a function of absolute magnitude for each field j by integrating the volume element as a function of the distance ℓ along the line of sight,

$$v_{\text{eff},j}(M_V) = \Omega_j \int\limits_{\ell_{-,j}(M_V)}^{\ell_{+,j}(M_V)} d\ell\, \ell^2 \nu_j[z(\ell)] \exp\left[\frac{-R(\ell) - R_0}{H}\right]. \tag{3.4}$$

Here the integration limits $\ell_{\pm,j}(M_V)$ for the jth field are determined from the sensitivity limits in Table 1, assuming that the color-mag relation holds exactly with no intrinsic scatter and no errors. The density function $\nu(z)\exp[-(R-R_0)/H]$ is computed according to equation (3.2) and using the parameters given in Table 2. Next, we form the total effective volume from all fields, $v_{\text{eff}} = \sum_j v_{\text{eff},j}$. Finally, we divide the total number of stars in a given magnitude bin by the effective volume integrated over that bin. The results are shown as crosses in Figure 2.

We note that this method takes account of neither Malmquist bias nor observational errors. However, as we argued in Paper I, Malmquist bias is not a significant problem for the *HST* survey because it extends to the "top" of the disk. In fact, one sees from Figure 2 that this simple binning procedure agrees quite well with the more sophisticated fit over most of the LF. We show the last four mags in individual 1-mag bins. We show (Poisson) error bars for these only to avoid clutter. At the faint end, Poisson errors are a potentially much more serious problem than Malmquist bias. We see from Figure 2 that the dip at $M_V = 15.5$ could plausibly be a statistical deviation from an intrinsically smooth LF. When transforming to a mass function, we therefore consider both the maximum-likelihood and naive-binning determinations.

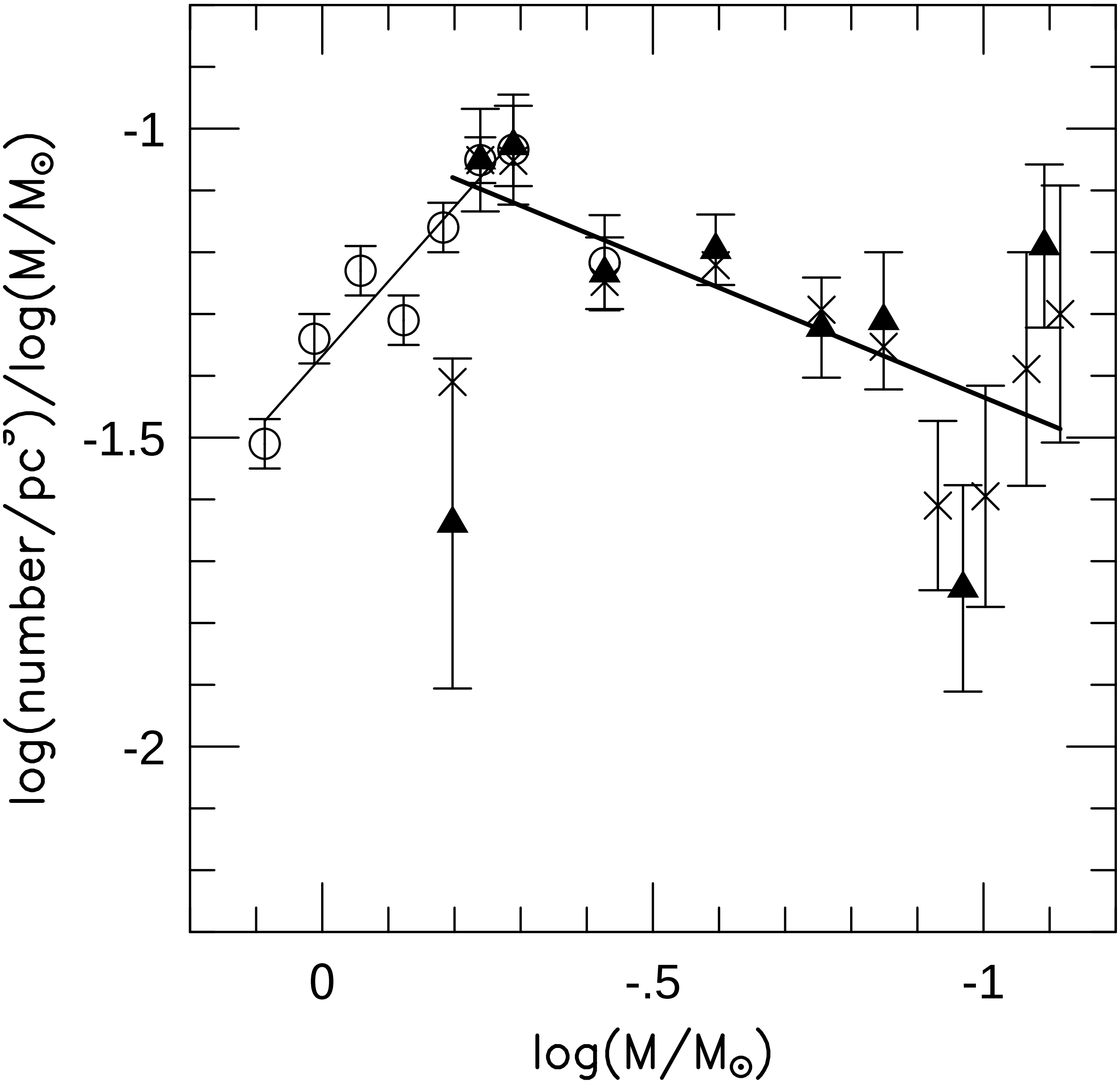

Figure 3. MFs derived from LFs on the basis of the mass-M_V relation of Henry & McCarthy (1993). Triangles and crosses show maximum-likelihood and naive-binning fits as in Fig. 2. Circles show MF based on the LF of Wielen et al. (1983) over the range $4 \le M_V \le 11$. The first 7 points for larger masses are well fit by the indicated straight line, $\Phi \equiv dN/d\log M = -1.37 - 1.21\,\log(M/M_\odot)$ for $M > 0.6\,M_\odot$. The *HST* crosses and the three relevant points from Wielen et al. (1983) are well fit by the other straight line, $\Phi = -0.99{+}0.44\,\log(M/M_\odot)$ for $M < 0.6\,M_\odot$. Thus the power-law index changes by 1.65 at $M \sim 0.6\,M_\odot$.

3.4. Mass Function

As in Paper I (see § 4.1), we adopt the empirical mass-M_V relation of Henry & McCarthy (1993). This relation is also in good agreement with the theoretical results of Baraffe & Chabrier (1996). In Figure 3 we show the mass functions derived from the LF using maximum likelihood (triangles) and naive binning (crosses). Also shown (circles) is the MF derived from the LF of Wielen, Jahreiss, & Krüger (1983) on the basis of parallax stars in the range $4 \le M_V \le 11$.

The most important feature of Figure 3 is the break in the power law at $M \sim 0.6\,M_\odot$. The straight line to the left is a linear (i.e., power-law) fit to the first seven points from the Wielen et al. (1983) data. The line to the right is a linear fit to the *HST* data (crosses). The respective slopes are -1.21 and 0.44. If the rising Salpeter-like slope to the left had remained unbroken, the four lowest mass bins would be ~ 20 times more populated. That is, they would contain ~ 500 stars rather than the 25 actually observed.

The break in the power law is not an artifact of the difference in surveys. Note that the last three points of the Wielen et al. (1983) data which correspond to magnitude bins $M_V = 9$, 10 , and 11, agree well with the *HST* data. This is true not only in the mean (which is an effect of using the parallax-star LF in this region to determine the overall normalization) but also in their individual values.

Note that the falling power-law is a reasonable fit to all of the naively binned data points (crosses). This suggests that the dip in the LF at $M_V = 15.5$ ($\log[M/M_\odot] \sim -0.1$) could plausibly be a statistical fluctuation. Nevertheless, the dip in the MF function is not purely an artifact of the maximum likelihood method since it is reproduced (albeit with reduced intensity) by the naively binned data. The sample is not large enough to determine if this dip is real.

3.5. Binary Correction

The *HST* data are sensitive to binaries with separations $\gtrsim 0.''3$ which, at typical distances of $\sim 2\,$kpc, corresponds to projected separations $\gtrsim 600\,$AU. Since only 1–2% of stars have binary companions in this range (Gould et al. 1995), while half or more of all stars are in binaries, the *HST* sample misses essentially all secondaries in binary systems.

We can make an empirical estimate of the incompleteness due to missed secondaries using the results of Reid et al. (1995). Reid et al. divided nearby M stars into two groups: (1) primaries and isolated stars, and (2) secondaries. (See also fig. 2 of Paper I). The nearby sample should be relatively complete because the stars are studied both photometrically and spectroscopically. For early M dwarfs

($M_V \leq 11$, $\log(M/M_\odot) > -0.4$), about 10% of stars are secondaries and so would be missed by *HST*. For late M dwarfs ($M_V \geq 15$, $\log(M/M_\odot) < -0.9$), about half are secondaries. Thus, incorporating the missing secondaries should change the slope from 0.44 to ~ 0.1. While this correction is admittedly crude, it is clear that missing binary companions cannot account for the break in power law.

3.6. Disk Mass

Our estimate for the total column density of M stars remains unchanged from Paper I (see Table 2) and therefore so does our estimate of the total column density of the disk: ($\Sigma \simeq 40\,M_\odot\,\mathrm{pc}^{-2}$). As we noted there, this is significantly lower than all published estimates of the dynamical mass of the disk. If one were to assume that the observed mass function (see Fig. 3) continues into the brown dwarf regime with slope α and normalized by twice the value of the last point (to take account of binaries), then the total column density of brown dwarfs would be $\Sigma_{\mathrm{BD}} = 6M_\odot/(1+\alpha)$. For $\alpha \sim 0$, this would bring the disk column density into line with the lowest dynamical estimate (Kuijken & Gilmore 1989), but not with most others (e.g. Bahcall 1984; Bienaymé, Robin, & Crézé 1987; Bahcall, Flynn, & Gould 1992; Flynn & Fuchs 1994). To reach the highest estmate of $\sim 80\,M_\odot\,\mathrm{pc}^{-2}$ (Bahcall et al. 1992) would require a dark component of $\sim 40\,M_\odot\,\mathrm{pc}^{-2}$ which would be produced, for example, by $\alpha = -2$ and a cutoff at $M = 0.01\,M_\odot$.

3.7. Microlensing

The optical depth to microlensing toward the Large Magellanic Cloud (LMC, $b = -33°$) of a general disk distribution $\rho(z)$ is given by $\tau = \csc^2 b \int_0^\infty dz\, 4\pi G\rho(z)z/c^2$. For a sech^2 and exponential distributions, this becomes $\tau = 2(\ln 2)\pi G\Sigma h \csc^2 b/c^2$, and $\tau = 2\pi G\Sigma h \csc^2 b/c^2$, respectively. Using these formulae and the parameter values given in Table 2, and assuming that the total column density of stars is $\Sigma_{\mathrm{tot}} = 2.1\Sigma_M$ (see Paper I), we estimate that the optical depth due to disk stars is $\tau \sim 8 \times 10^{-9}$, a factor of 25 lower than the most recent estimate for the observed optical depth $\tau \sim 2 \times 10^{-7}$ by the MACHO collaboration (Alcock et al. 1996).

We note that the MACHO collaboration's very high magnification event (number 5 in Alcock et al. 1996) could well be due to a disk star. The color and magnitude of the unlensed light in this event are inconsistent with the characteristics of any known population in the LMC, but are consistent with a foreground late M dwarf within the seeing disk of the lensed source (an LMC main-sequence star). The probability of finding an M dwarf in a randomly chosen seeing disk is small, but an M dwarf would be the most likely stellar type recovered in this way if the lens were a disk foreground star.

The break in the slope of the MF shown in Figure 3 has important implications for the interpretation of microlensing toward the Galactic Bulge. Zhao, Spergel, & Rich (1995) have shown that the bulge event rate would be well explained if all of the dynamically-measured bulge mass ($\sim 2 \times 10^{10} M_\odot$) were in a Salpeter MF ($\alpha = -1.35$) over the range $0.08 M_\odot \leq M \leq 0.6 M_\odot$. That is, the events could be explained without recourse to brown dwarfs or other dark matter. The bulge LF has now been measured down to $V = 26$ ($M_V \sim 10$ or $M \sim 0.5\, M_\odot$) by Light, Baum, & Holtzman (1996) and these observed stars account for $\sim 1 \times 10^{10} M_\odot$ of the bulge mass but very few of the lensing events (Han 1996). The shape of the observed bulge LF is consistent with that of the disk LF over the same range and is therefore consistent with a Salpeter MF. Han & Gould (1995) showed that a Salpeter MF explains the bulge events provided that it is extended to $\sim 0.05\, M_\odot$, i.e., includes a substantial number of brown dwarfs. The low-mass end of the disk MF is, however, inconsistent with a Salpeter MF (see Fig. 3). While the agreement between disk and bulge LFs in the region where they are both observed is no guarantee of their agreement at fainter mags, similar LFs (and therefore MFs) does appear to be the simplest hypothesis. If the bulge MF is extended using the estimate for the disk MF given in Paper I, then the observed+inferred bulge stellar population accounts for $1.4 \times 10^{10} M_\odot$, i.e. $\sim 70\%$ of the dynamical estimate, but these stars still account for only a small fraction of the observed microlensing events. Han (1996) finds that the remaining $\sim 30\%$ must be in brown dwarfs to explain the observed events. In brief, if current estimates of the lensing rate toward the bulge are confirmed then either: 1) the bulge and disk mass functions are very different for $0.1\, M_\odot \leq M \leq 0.5\, M_\odot$ or 2) the bulge contains a large population of brown dwarfs.

4. Future Prospects

There are two types of additional observations that would significantly improve our understanding of disk M dwarfs. The first is to acquire more statistics, particularly for late M dwarfs. We have demonstrated the existence of a break in the power law of the disk MF near $M \sim 0.6\, M_\odot$. However, more data are required to investigate the detailed structure of the MF. A large body of suitable *HST* WFC2 observations have already been made and we are in process of analyzing these. More observations are expected in the future.

Second, the Groth Strip offers a unique opportunity for ground-based follow-up observations. In most cases, it is not efficient to observe individual deep WFC2 fields from the ground because of the $\mathcal{O}(10^2)$ mis-match in field sizes. One consequence of this mis-match is that there are no empirical calibrations of the *HST* filters for late M dwarfs. The Groth Strip contains over 50 disk M dwarfs (plus an equal number of spheroid M dwarfs) and would therefore provide an excellent empirical check on the calibration of Bahcall et al. (1994) which was determined by convolving the *HST* filter functions with ground-based spectra. In addition, deep BVI observations would allow one to measure the B excess (at fixed $V-I$) of each star in the field and so estimate the degree to which any of the stars may be sub-luminous. This would permit more sophisticated modeling of the luminosity of stars than the single color-mag relation used here. At present, there are no data to form the basis for such modeling and theoretical estimates are too uncertain to be of use. It would be possible to make such observations in non-*HST* fields and P. Boeshaar (private communication, 1996) is carrying out a study of this type. However, observation of the Groth Strip has the important advantage that the stars are already identified unambiguously. In addition, as mentioned above, these observations would be very valuable for calibration of the *HST* filters.

Acknowledgements: A. G. was supported in part by NSF grant ast 9420746 and in part by NASA grant NAG5-3111. J. N. B. was supported by NASA grant NAG5-1618. The work is based in large part on observations with the NASA/ESA Hubble Space Telescope, obtained at the Space Telescope Science Institute, which is operated by the Association of Universities for Research in Astronomy, Inc. (AURA), under NASA contract NAS5-26555. Important supplementary observations were made at KPNO and CTIO operated by AURA.

REFERENCES

Bahcall, J. N. 1984, ApJ, 276, 169

Bahcall, J. N. 1986, ARA&A, 24, 577

Bahcall, J. N., Flynn, C., & Gould, A. 1992, ApJ, 389, 234.

Bahcall, J. N., Flynn, C., Gould, A., & Kirhakos, S. 1994, ApJ, 435, L51.

Baraffe, I., & Chabrier, G. 1996, ApJ, 461, L51

Bienaymé, O., Robin, A., & Crézé, M. 1987, A&A, 180, 94

Burstein, D. & Heiles, C. 1984, AJ, 90, 817

Cowley, A. P., & Hartwick, F. D. A. 1991, ApJ, 373, 80

Dahn, C. C., Liebert, J. W., & Harrington R. S. 1986, AJ, 91, 621

Dahn, C. C., Liebert, J. W., Harris, H., & Guetter, H. C. 1995, p. 239, An ESO Workshop on: the Bottom of the Main Sequence and Beyond, C. G. Tinney ed. (Heidelberg: Springer)

Flynn, C. & Fuchs, B. 1994, MNRAS, 270, 471

Flynn, C. & Gould, A., & Bahcall, J. N., 1996, ApJ, 466, L55

Gould, A., Bahcall, J. N., & Flynn, C. 1996, ApJ, 465, 759

Gould, A., Bahcall, J. N., Maoz, D., & Yanny, B. 1995, ApJ, 441, 200

Han, C. 1996, ApJ, submitted

Han, C. & Gould, A. 1996, ApJ, 467, 540

Henry, T. J. & McCarthy, D. W. 1993, AJ, 106, 773

Kuijken, K. & Gilmore, G. 1989, MNRAS, 239, 605

Light, R. M., Baum, W. A., & Holtzman, J. A. 1996, in preparation

Monet, D. G., Dahn, C. C., Vrba, F. J., Harris, H. C., Pier, J. R., Luginbuhl, C. B., & Ables, H. D. 1992, AJ, 103, 638

Reid, I. N. 1991, AJ, 102, 1428

Reid, I. N., Hawley, S. L., & Gizis, J. E. 1995, AJ, 110, 1838

Williams, R. E., et al. 1996, AJ, 112, 1335

Wielen, R., Jahreiss, H., & Krüger, R. 1983, IAU Coll. 76: Nearby Stars and the Stellar Luminosity Function, A. G. D. Philip and A. R. Upgren eds., p 163